Surface & Coatings Technology 412 (2021) 127015

Contents lists available at ScienceDirect

Surface & Coatings Technology

journal homepage: www.elsevier.com/locate/surfcoat

Novel utilization of powder-suspension hybrid feedstock in HVAF spraying to deposit improved wear and corrosion resistant coatings

Satyapal Mahade [a,*], Lidia Baiamonte [a,b], Esmaeil Sadeghimeresht [a], Stefan Björklund [a], Francesco Marra [b], Shrikant Joshi [a]

[a] Department of Engineering Science, University West, Sweden,
[b] Department of Chemical Engineering Materials Environment, Sapienza University of Rome, Italy

ARTICLE INFO

Keywords:
Inconel-625
Chromium carbide
Suspension
High velocity air fuel
Corrosion
Wear

ABSTRACT

Deployment of a suspension feedstock has been known to alleviate problems associated with using sub-micron and nanosized powder feedstock for thermal spraying of monolithic as well as powder-suspension 'hybrid' composite coatings. However, a powder-suspension hybrid feedstock has never been previously used in high-velocity air-fuel (HVAF) spraying. In this work, for the very first time, a chromium carbide (Cr_3C_2) suspension has been co-sprayed along with an Inconel-625 (IN-625) powder by the HVAF process as an illustrative case study. Two variants of the IN-625 + Cr_3C_2 hybrid coatings were produced by varying relative powder-suspension feed rates. For comparison, pure IN-625 coating was also deposited utilizing identical spray parameters. Detailed microstructural characterization, porosity content, hardness measurement and phase analysis of the as-deposited coatings was performed. The suspension-derived carbides were retained in the bulk of the coating, resulting in higher hardness. In the dry sliding wear test, the hybrid coatings demonstrated lower wear rate and higher coefficient of friction (CoF) compared to the conventional, powder-derived IN-625 coatings. Furthermore, the wear rate improved slightly with an increase in Cr_3C_2 content in the hybrid coating. Post-wear analysis of the worn coating, worn alumina ball and the wear debris was performed to understand the wear mechanisms and material transfer in the investigated coatings. In the potentiodynamic polarization test, higher corrosion resistance for hybrid coatings than conventional IN-625 coatings was achieved, indicating that the incorporation of a secondary, carbide phase in the IN-625 matrix did not compromise its corrosion performance. This work demonstrates a novel approach to incorporate any finely distributed second phase in HVAF sprayed coatings to enhance their performance when exposed to harsh environments.

1. Introduction

Protective coatings are utilized in vast majority of applications to enhance the performance and durability of engineering components. Thermal spray is a versatile processing route, which is usually employed to deposit protective coatings on components for mitigating wear, corrosion etc. During thermal spraying, adequate thermal and kinetic energy is imparted to the feedstock, which eventually deposits as a splat onto the substrate. Thermal spray route such as High Velocity Air Fuel (HVAF) involves lower processing temperature than plasma spray and high velocity oxy-fuel (HVOF) processes, which is beneficial in depositing temperature-sensitive carbide-based materials [1,2]. In general, all the above thermal spray processes have limitations in processing sub-micron and nano-sized feedstock due to problems associated with their feeding [1,3]. Liquid feedstock utilizing such fine-sized powder suspended in solvents like water or ethanol overcomes the above challenges [4,5]. Recently, HVOF and plasma processed 'hybrid' coatings deposited by simultaneous injection of powder-suspension hybrid feedstocks yielded superior wear resistance than conventional coatings [6–9]. Although never previously attempted, such hybrid spraying could also be an interesting approach to explore in an HVAF and constitutes the main focus of this study.

Inconel-625 (IN-625) is known for its excellent high temperature mechanical properties and corrosion resistance [10–12]. Thermally sprayed IN-625 coatings are extensively used in marine and chemical industries to impart corrosion resistance [13,14]. However, one drawback of IN-625 is that it lacks adequate wear resistance, thus limiting its in-service durability [13]. On the other hand, carbide-based coatings

* Corresponding author.
E-mail address: satyapal.mahade@hv.se (S. Mahade).

https://doi.org/10.1016/j.surfcoat.2021.127015
Received 24 December 2020; Received in revised form 16 February 2021; Accepted 21 February 2021
Available online 27 February 2021

possess excellent wear resistance [4,15–17]. 3However, they are prone to inflight oxidation during plasma spraying, which can compromise their wear and corrosion performance [18,19]. In the past, laser cladding of IN625 + Cr_3C_2 composite was reported to enhance the wear resistance compared to the conventional IN-625 coating [11,20]. Similar IN625 + Cr_3C_2 combinations have also been used in coatings sprayed by HVOF and HVAF [21,22]. Furthermore, thermally sprayed, carbide-based coatings deposited using finer feedstock (<10 μm) demonstrated excellent wear resistance due to homogenous distribution of carbides in the tougher metallic matrix [4,18,23].

Although two patents refer to utilization of suspensions/liquid injection with HVAF [24,25], no publications are available on the subject. For the first time, this work aimed at exploring the feasibility of powder-suspension hybrid feedstock spraying by HVAF. As a case study, IN-625 was chosen as the matrix system due to its attractive corrosion properties, while chromium carbide was chosen as the reinforcing phase due to its excellent wear resistance. Hybrid spraying of IN-625 (conventional "coarse" spray-grade powder) + Cr_3C_2 (suspension of "fine" powders) was attempted utilizing HVAF process. For comparison, a conventional, powder-derived IN-625 coating was also deposited utilizing identical HVAF spray conditions. The as-deposited coatings were comprehensively characterized and their wear and corrosion behavior was also assessed.

2. Experimental work

Mild steel substrates (SSAB Domex® 355, Sweden) of 1 in. diameter and 6 mm thickness were grit blasted using alumina to achieve a surface roughness Ra of approximately 3.5 μm. Inconel-625 (AMPERIT® 380.065, Höganäs Germany GmbH) powder with a particle size of −30 + 10 μm and an experimental, water-based Cr_3C_2 (D_{50} 4 μm) suspension, with 40 wt% solid load provided by Treibacher Industrie AG, Austria were used for coating deposition. A 4L4 M3 nozzle and an M3™ supersonic torch (UniqueCoat, US) was used both to spray the powder alone as well as a simultaneously injected powder-suspension hybrid feedstock combination to deposit conventional and hybrid coatings by the HVAF process The torch passing speed was kept at 100 m/min with a 5 mm/step to deposit conventional and hybrid coatings. A commercially available UniqueCoat Powder injector type #3, equipped with a powder hose of 6 mm outer diameter and 4 mm inner diameter, was used. A commercially available, Nanofeed suspension feeder (Northwest Mettech Corp., Canada) with a 3/16 in. nylon hose, was used for the carbide suspension injection to process hybrid coatings. Downstream of the 100 mm long injector tube, the powder along with 60 l/m carrier gas, and the suspension were mixed via a T-joint and allowed to exit the powder injection tube together in the same manner as in case of conventional powder feed, as clearly illustrated in the schematic shown in Fig. 1 Two variants of the IN625 + Cr_3C_2 hybrid coatings, referred to as 'Hybrid-1' (IN625 + 46wt%Cr_3C_2) and 'Hybrid-2' (IN625 + 35wt%Cr_3C_2), along with reference IN-625 coating, were deposited. The spray parameters used to deposit the conventional and hybrid coatings are reported in Table. I. For the hybrid coatings, the powder feed-rate was kept half of the conventional coating in order to accommodate the suspension derived carbides in the matrix. There was no evident difference in deposition rate and deposition efficiency in case of the hybrid coatings and the conventional coating, thereby suggesting that the introduction of the carbide in suspension form did not significantly influence coating deposition. Microstructural examination was performed using SEM (TM300, Hitachi, Japan)/EDS (Bruker, Germany). Porosity content was analyzed by image analysis ('ImageJ' [26]) using fifteen different high magnification (3000×) SEM micrographs. Micro-indentation tests were performed at 1.96 N load (0.2 kgf) on the polished coating cross sections using HMV-2 series micro hardness tester (SHIMADZU Corp., Japan). XRD analysis was performed on as-deposited coating specimens using a PANalytical X'Pert3 diffractometer, operating at 40 KV and 40 mA with Cu Kα1 radiation. The scan range was 20–80° (2θ), with a step size of 0.02° and counting time of 2 s. Ball-on-disc tests were performed according to ASTM-G99 standard [27] using a tribometer (TRB3, Anton Paar, Netherlands). The coated specimens were polished to a surface roughness of Ra < 0.2 μm prior to the ball-on-disc test. Alumina balls (ST instruments, Netherlands) of 6 mm diameter were used as the counter surface. After initial trials, a normal load of 1 N, linear velocity of 20 cm/s and a sliding distance of 500 m were chosen and the test was repeated on three coated test specimens for each coating condition. The volume loss in the coating was measured using white light interferometer (Profilm 3D, Filmetrics, Germany). Specific wear rate of the coatings was calculated according to Eq. (1) and reported in [mm^3/(N·m)].

$$\textit{Specific wear rate}\ \left[mm^3/(N.m)\right] = \frac{\text{Volume}\ [mm^3]}{\text{Normal load [N]Sliding distance[m]}} \quad (1)$$

Corrosion tests were also conducted on all coatings using a 3.5 wt% NaCl solution at room temperature. A standard three electrode system, including a graphite counter electrode, a saturated Ag/AgCl reference electrode, and the coated sample as the working electrode was used. The surface area of the coated specimens exposed to the test solution was 2.5 cm^2. The surface of the specimens was mirror polished (Ra <0.1 μm) prior to testing to obtain a smooth and defect free surface. The coated specimens were immersed in the test solution for 7200 s to achieve a

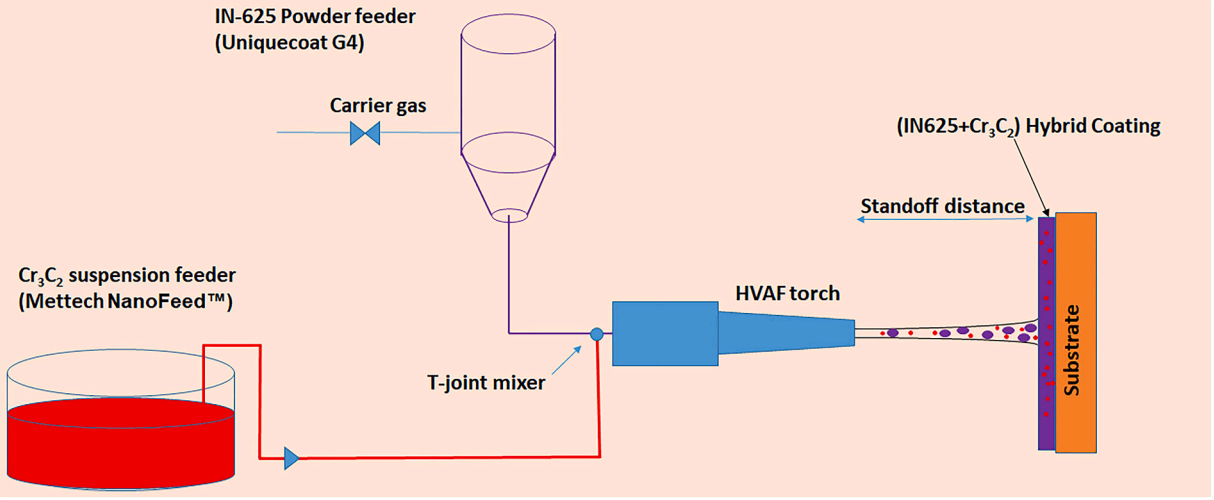

Fig. 1. Illustration of the powder-suspension injection by HVAF to deposit hybrid coating microstructure.

Table I
HVAF spray parameters utilized to deposit IN-625, Hybrid-1 and Hybrid-2 coatings.

Coating ID	Air (psi)	Fuel 1 (psi)	Fuel 2 (psi)	Carrier gas (l/min)	Powder feed rate (g/min)	Suspension feed rate (ml/min)	Standoff distance (mm)	Coating thickness per pass (μm)	No. Spray passes
IN-625	111	100	105	60	100	0	350	26	11
Hybrid-1	111	100	105	60	50	110	350	13	23
Hybrid-2	111	100	105	60	50	70	350	13	23

stable potential. Potentiodynamic polarization tests were then performed using a Gamry instrument (Reference 3000, Pennsylvania, US). The test specimens were excited from −0.3 to 1.3 V Ag/AgCl at a scanning rate of 0.16 mV/s. Electrochemical parameters, such as corrosion potential (E_{corr}), corrosion current density (i_{corr}), cathodic Tafel slope (β_c), and anodic Tafel slope (β_a) were obtained to calculate the polarization resistance (R_p), according to Eq. (2):

$$R_p = \frac{\beta_a \beta_c}{2.303 i_{corr}(\beta_a + \beta_c)} \quad (2)$$

3. Results and discussion

3.1. Microstructural analysis

SEM analysis of IN-625 powder feedstock showed spherical particles with diameter ranging from −30 + 10 μm, according to Fig. 2(a). Satellite-like features on the surface of spherical IN-625 powder could also be seen in Fig. 2(b). The EDS analysis of IN-625 powder feedstock is shown in Table II. In the case of Cr_3C_2, irregular shaped particles with particle size <4 μm were seen in Fig. 2(c).

The cross-sectional SEM micrograph of the IN-625 coating in Fig. 3 (a) showed a dense microstructure, with a delamination-free interface with the substrate. Higher magnification SEM micrograph of the cross-section in Fig. 3(b) showed visible, fine pores. The top surface SEM micrograph of IN-625 showed plastically deformed splats with a range of sizes corresponding to different particle sizes present in the powder according to Fig. 3(c).

The cross-sectional SEM micrograph of Hybrid-1 coating also showed a dense, delamination-free microstructure in Fig. 3(d). In the coating's bulk, carbides appear as dark phase embedded in the IN-625 coating matrix according to Fig. 3(e). The top surface view SEM micrograph in Fig. 3(f) showed the presence of plastically-deformed and undeformed splats. The Hybrid-2 coating also showed largely similar microstructure in Fig. 3 (g, h, i), where presence of carbides (dark phase) was clearly visible in Fig. 3(h), and the minor difference (in Vol%) in suspension derived carbides in Hybrid-1 and Hybrid-2 coating is not readily discernible.

High magnification SEM/EDS analysis of the dark phase in the cross section of Hybrid-1 coating confirmed the presence of 'Cr' and 'C' from the elemental maps, according to Fig. 4, indicating that they were derived from the suspension feedstock. Furthermore, the elemental quantification of dark regions (Spectrum 1, 2) showed 'Cr' content of approximately 88 wt% and 12 wt% 'C', see Table III, confirming the retention of suspension-derived feedstock in the as-deposited coating. On the other hand, the brighter region (Spectrum-3) showed constituent alloying elements of IN-625. Image analysis of the cross-sectional SEM micrographs (2000 x magnification) considered from the coating's bulk revealed the volume fraction of carbide phase content in Hybrid-1 to be 4.1 ± 0.5 vol% whereas the Hybrid-2 coating showed a carbide content of 2.7 ± 0.9 vol%. Higher carbide phase content retained in Hybrid-1 than Hybrid-2 can be attributed to the relatively higher suspension feed rate employed in case of the former, see Table I. It can also be seen that the amount of carbide feedstock retained in both the hybrid coatings was too low compared to the initial carbide content of 46 wt% (Hybrid-1) and 35 wt% (Hybrid-2) utilized during hybrid spraying. It should be mentioned that the processing temperature of hybrid coatings by HVAF is lower than the melting temperature of Cr_3C_2. Furthermore, the brittle nature of Cr_3C_2 does not allow plastic deformation of the carbide as in the case of IN-625. Therefore, it is expected that Cr_3C_2 retains its feedstock size (<5 μm) in the HVAF processed hybrid coatings. Additionally, the carbide phase appears predominantly in clusters rather than distributed uniformly throughout the coating, according to Fig. 3(e and f). The uneven distribution of Cr-based carbides could perhaps be attributed to the high back pressure in the HVAF torch that needs to be surmounted during suspension feeding. The authors' group is currently exploring a modified suspension delivery set up to overcome the above challenge.

Table II
EDS analysis of IN-625 powder feedstock.

Element	Wt%
Ni	63.1
Cr	22
Mo	9.1
Nb	3.9
Ta	<1
Co	<1
Fe	<1

In the top surface SEM micrograph of as-deposited Hybrid-1 coating shown in Fig. 5(a), 'Cr'-rich regions are seen but corresponding 'C' enrichment is not obvious and precludes confirmation of these being the suspension derived carbides. Instead, well-distributed 'Cr', 'Ni' and other constituent elements from the original IN-625 composition could be seen. However, the suspension-derived carbides were visible upon polishing the coated surface, according to the top surface SEM micrograph shown in Fig. 5(b) and its corresponding EDS elemental maps.

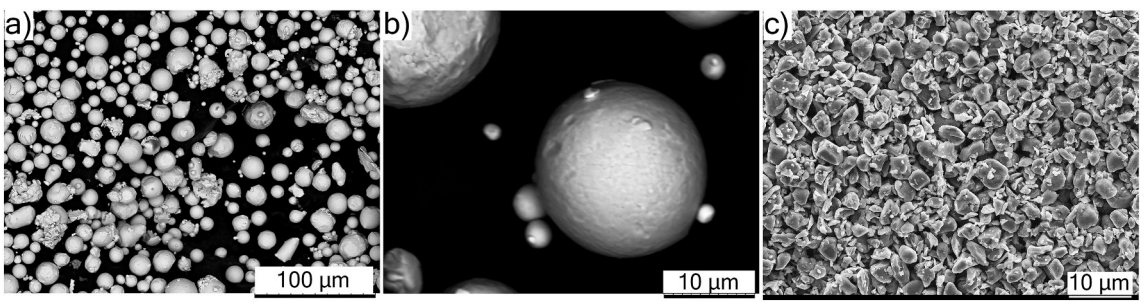

Fig. 2. SEM micrographs of the different feedstocks a) IN625 b) higher magnification IN625 c) Cr_3C_2.

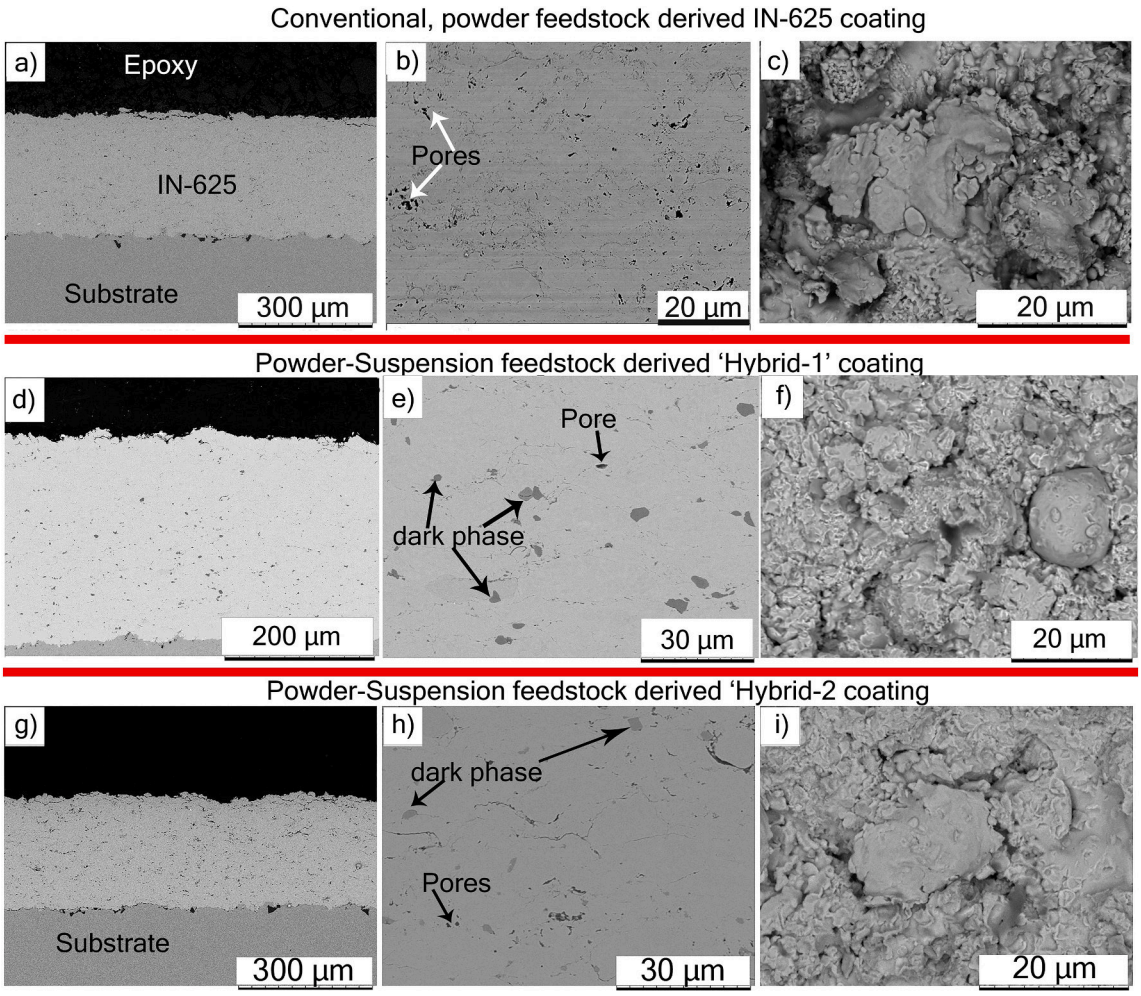

Fig. 3. SEM/EDS analysis of (a, b) IN625 - cross section c) IN625 - top surface (d, e) Hybrid-1 -cross section f) Hybrid −1 - top view (g, h) Hybrid-2 cross section i) Hybrid-2 top view.

During HVAF processing of hybrid coating, Cr_3C_2 cannot undergo plastic deformation. Therefore, it is plausible that the Cr_3C_2 particles tend to impact the coating surface and bounce off, unless either "buried" by the subsequent impact of IN625 particles or "captured" by an oncoming IN-625 particle before bouncing off. Based on the microstructural analysis results, the plausible mechanism of formation of hybrid coating microstructure of HVAF-processed IN-625 + Cr_3C_2 is shown in Fig. 6. Additionally, only Cr_3C_2 suspension feedstock spraying by HVAF directly on a Domex steel substrate (but not on as-sprayed IN625) was attempted. However, no material build-up was observed in the cross sectional and top surface SEM analysis of Cr_3C_2 suspension sprayed by HVAF, although few fragmented particles (Cr_3C_2) were observed. These results appear to support the above mechanism.

3.2. Porosity content and micro-hardness

The porosity content of HVAF-processed hybrid coatings and IN-625 coatings was comparable and less than 3%, according to Fig. 7(a). It should be mentioned that, particularly for wear and corrosion applications, low porosity content in a coating is desirable; otherwise, the pores can serve as degradation initiation sites and result in inferior performance.

The micro-hardness results of IN-625 and hybrid coatings showed slightly higher hardness for the hybrid coatings compared to IN-625, according to Fig. 7(b). Among the hybrid coatings, the Hybrid-1 coating showed somewhat higher hardness than Hybrid-2 but, given the scatter in the measured hardness values, this difference cannot be deemed to be significant. In the case of hybrid coatings, compacting action and compressive stresses induced due to peening effect of the bounced-off Cr_3C_2 particles could have contributed to their somewhat higher mean hardness, in addition to the presence of Cr_3C_2 in the hybrid coating. Similar findings on improved hardness due to peening effect and incorporation of carbides were reported elsewhere [18,28]. Furthermore, the relatively higher variation in hardness measurement for hybrid coatings compared to the IN-625 coating, is indicative of somewhat inhomogeneous distribution of Cr_3C_2 in the matrix due to suspension feeding problems, as discussed in the subsequent section (Section 3.5).

3.3. XRD analysis

XRD analysis of chromium carbide feedstock showed orthorhombic Cr_3C_2 whereas the IN-625 feedstock showed predominantly 'Ni' matrix peaks, see Fig. 8(a, b). The surface XRD analysis of as-deposited (unpolished) IN-625, Hybrid-1 and Hybrid-2 coatings in Fig. 8(c) showed identical phase constitution, with Ni peaks slightly shifting in the case of hybrid coatings where Hyrbid-1 coating showed a peak shift of just under 0.5°, followed by Hyrbid-2 coating. The marginal peak shift in hybrid coatings could be attributed to incorporation of Cr_3C_2 in the IN625 matrix along with the compressive stresses induced by bounced-off Cr_3C_2 particles [11]. The absence of Cr_3C_2 peaks from the hybrid coatings is in agreement with un-polished top surface SEM/EDS results,

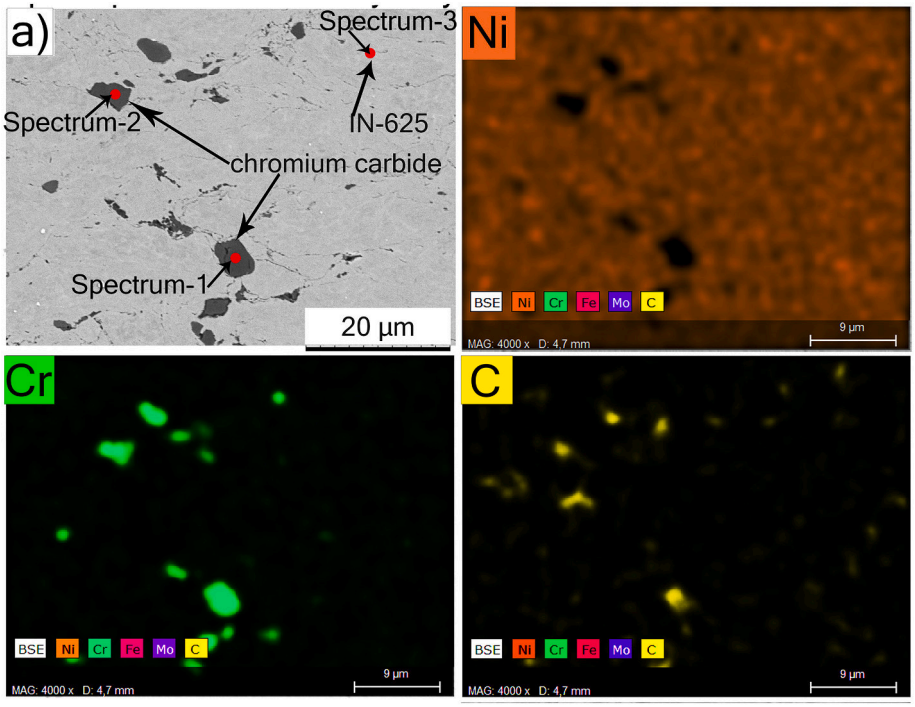

Fig. 4. SEM/EDS analysis of the cross section of Hybrid-1 coating and its corresponding elemental maps.

Table III
Quantitative EDS analysis performed in the cross section of as-deposited Hybrid-1 coating comprising chromium carbide (Spectrum 1 and 2) and IN625 matrix (Spectrum-3).

Element (wt%)	Spectrum-1	Spectrum-2	Spectrum-3
Ni	<1	<1	63.6
Cr	87.5	88.3	20.3
Mo	–	–	10.2
Nb	–	–	5.2
C	12.3	11.1	<1
Fe	–	–	<1

thereby supporting the hypothesis that Cr_3C_2 particles tend to bounce off unless captured by an oncoming IN625 particle, as illustrated in Fig. 5.

3.4. Sliding wear test

3.4.1. Specific wear rate and coefficient of friction

The Hybrid-1 coating had the lowest specific wear rate (1×10^{-4} $mm^3/N{\cdot}m$) whereas the IN-625 coating had the highest wear rate (1.8×10^{-4} $mm^3/N{\cdot}m$), according to Fig. 9(a). The ranking for specific wear rate of the investigated coatings are in agreement with their hardness results, where the higher hardness coating showed higher wear resistance. The higher Cr_3C_2 content in Hybrid-1 coating (approximately 4% in Vol.) than Hybrid-2 coating (approximately 3% in Vol.) led to its lower mean volume loss. It seems that the presence of a harder phase in a relatively ductile matrix results in minimizing material loss during sliding wear test. Furthermore, compressive stresses induced due to peening effect of the bounced-off Cr_3C_2 particles in the case of hybrid coatings could have also contributed to their improved wear performance. Similar findings related to improvement in wear performance were reported for plasma sprayed, carbide-laden hybrid coatings [18]. The coefficient of friction (CoF) evolution with sliding time is shown in Fig. 9(b). All the tested specimens showed steady state regime after approximately 800 s. Furthermore, the hybrid coatings showed slightly higher COF in the steady sate regime compared to IN-625 coatings. Although the presence of a harder reinforcement lowered the wear rate, it led to an increase in CoF. Similar finding were reported by Matikainen et al. for carbide-laden coatings where an increase in carbide content led to an increase in CoF and lower wear rates [29]. A detailed post-wear analysis can shed light on the wear mechanisms, material transfer etc. in the investigated coatings. Therefore, IN-625 coating and Hybrid-1 coatings were considered for post-wear analysis.

3.4.2. Post-wear analysis

3.4.2.1. Hybrid-1 coated specimen. SEM analysis of the surface of a ball-on-disc tested Hyrbrid-1 coating showed a well-distinguished wear track of approximately 550 µm width, according to Fig. 10(a). The wear track comprised distinct, bright and grey regions. High magnification SEM micrograph in the wear track showed the initiation site of splat failure, with visible cracks in the bright region, see Fig. 10(b). Higher magnification SEM micrograph in Fig. 10(c) and its corresponding EDS elemental maps showed 'Ni', 'Cr' in the bright regions whereas the grey region showed high 'O', 'Ni', 'Cr', 'Al' along with 'C', according to Table IV. The presence of 'C' indicates brittle fracture and pullout of carbides from the matrix due to cyclic stresses encountered during the testing. The presence of 'O' in the dark region confirms tribo-oxidation as one of the wear mechanisms. During the initial stages of the sliding wear test, some amount of wear debris generated from the coating surface and the alumina ball can be expelled out of the wear track and while some also gets trapped in the wear track. With the test progression, the trapped debris between the ball and the coating surface get finer. These fine wear particles eventually oxidize due to the frictional heat generated during the test, resulting in formation of tribo-oxides. Based on the composition, thickness and adhesion with the coated surface, the in-situ formed tribo-oxides during wear test can be beneficial in minimizing wear loss [30]. In general, the composition of the in-situ formed tribo-oxides depends on the coating composition, test conditions such as the applied normal load, sliding speed etc. [31]. The microcutting scars in the bright region of the wear track also suggests abrasive wear of the ductile IN-625 matrix. Furthermore, presence of 'Al' in the wear track confirms material transfer from the ball surface to the coating. Similar tribo-oxidation, abrasive wear and brittle fracture

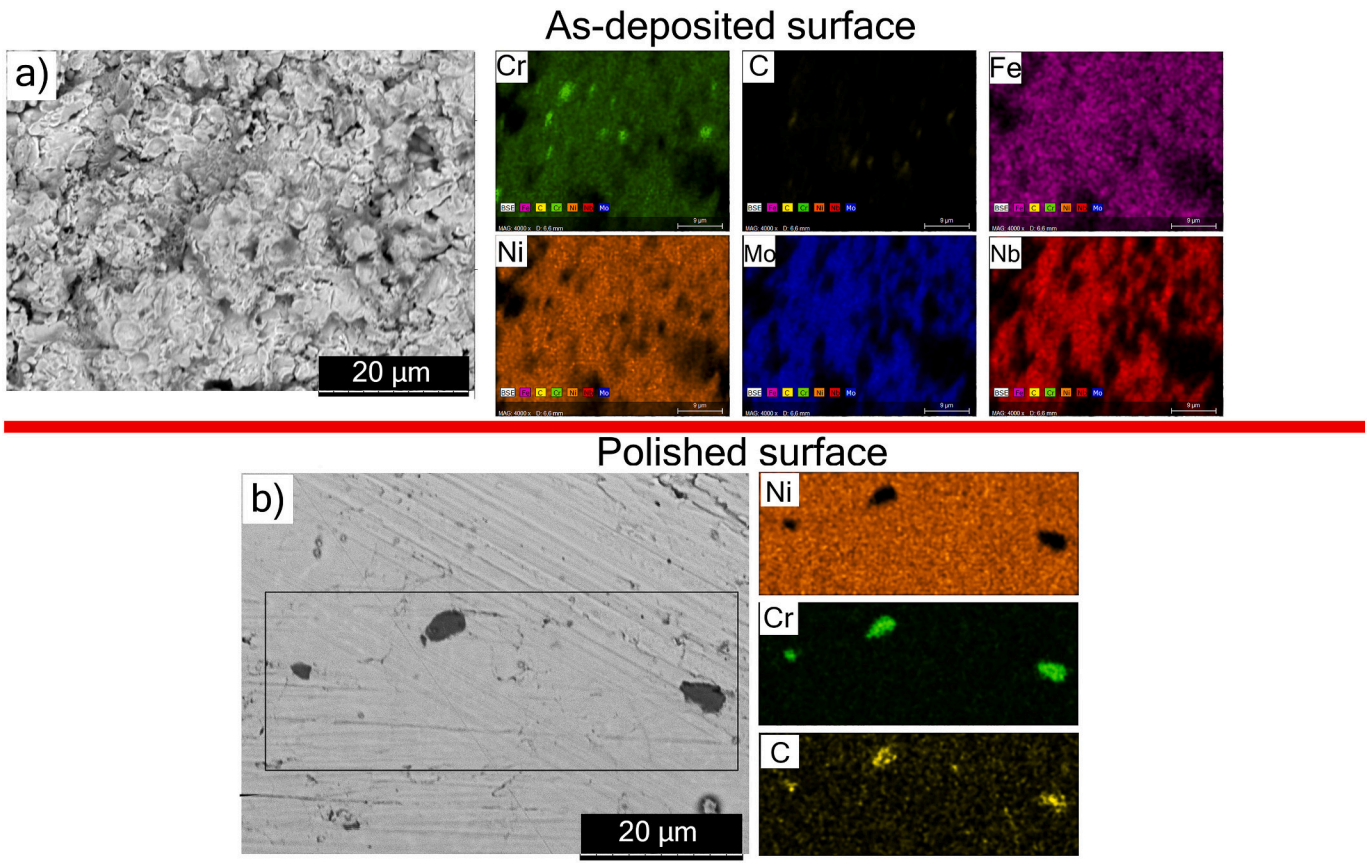

Fig. 5. SEM/EDS analysis of Hybrid-1 coating a) as-deposited top surface and its corresponding elemental maps b) polished top surface and its corresponding elemental maps.

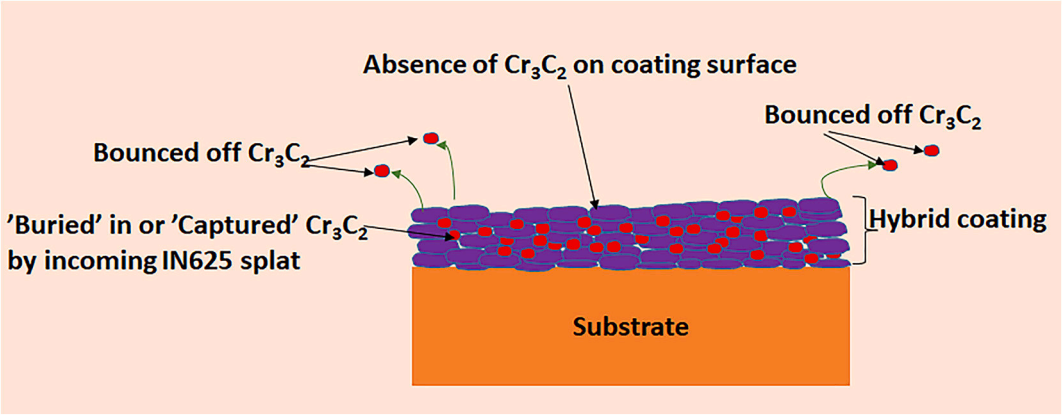

Fig. 6. Schematic illustration of the IN-625 + Cr_3C_2 hybrid coating microstructure when deposited by HVAF.

wear mechanisms were reported elsewhere for HVAF and HVOF sprayed, carbide containing coating compositions (Cr_3C_2-NiCr, WC-CoCr) [29,32,33].

The alumina ball wear scar showed a distorted circular shape, with a scar diameter of approximately 550 µm, which was similar to that of the wear track width on the coated specimen, according to Fig. 11(a). High magnification SEM micrograph in Fig. 11(b) and its corresponding EDS analysis of the worn region showed 'Ni' and 'Cr' in the wear track, confirming material transfer from the coated specimen to the ball surface. During the initial stage of sliding wear test, the ball surface and the coated specimen have a point contact. With the test progression, the contact between the ball and the coated specimen becomes circular. However, the expelled debris accumulates in the vicinity of the wear track and tends to enter the contact region between the ball and the coated specimen, leading to distortion of the circular scar shape.

Wear debris collected from the wear track and its adjacent region comprised coarse and fine-sized particles, according to Fig. 12(a). The coarser particles were in the size range of 10–20 µm in length whereas the finer particles were < 2 µm, according to Fig. 12(b). Elemental analysis of the wear debris revealed presence of 'Cr', 'Ni', and 'Al', indicating material loss from the coating and ball surface. Presence of 'O' in the finer debris suggests in-situ formed tribo-oxides, which were also seen in the coating wear track. On the other hand, the elemental map of coarse-sized debris shows absence of 'O', indicating that the

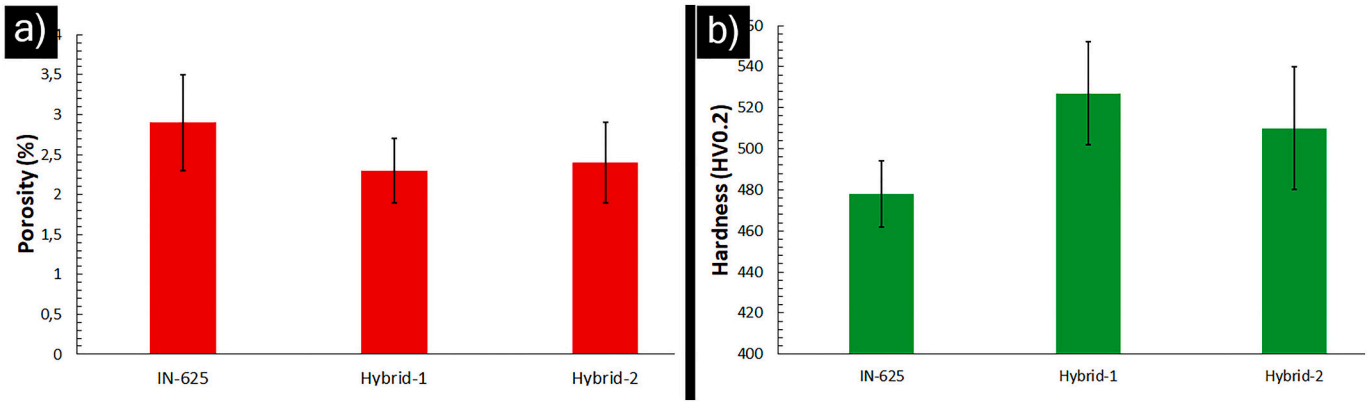

Fig. 7. a) Porosity content of the as-deposited coatings b) Hardness of the as-deposited coatings.

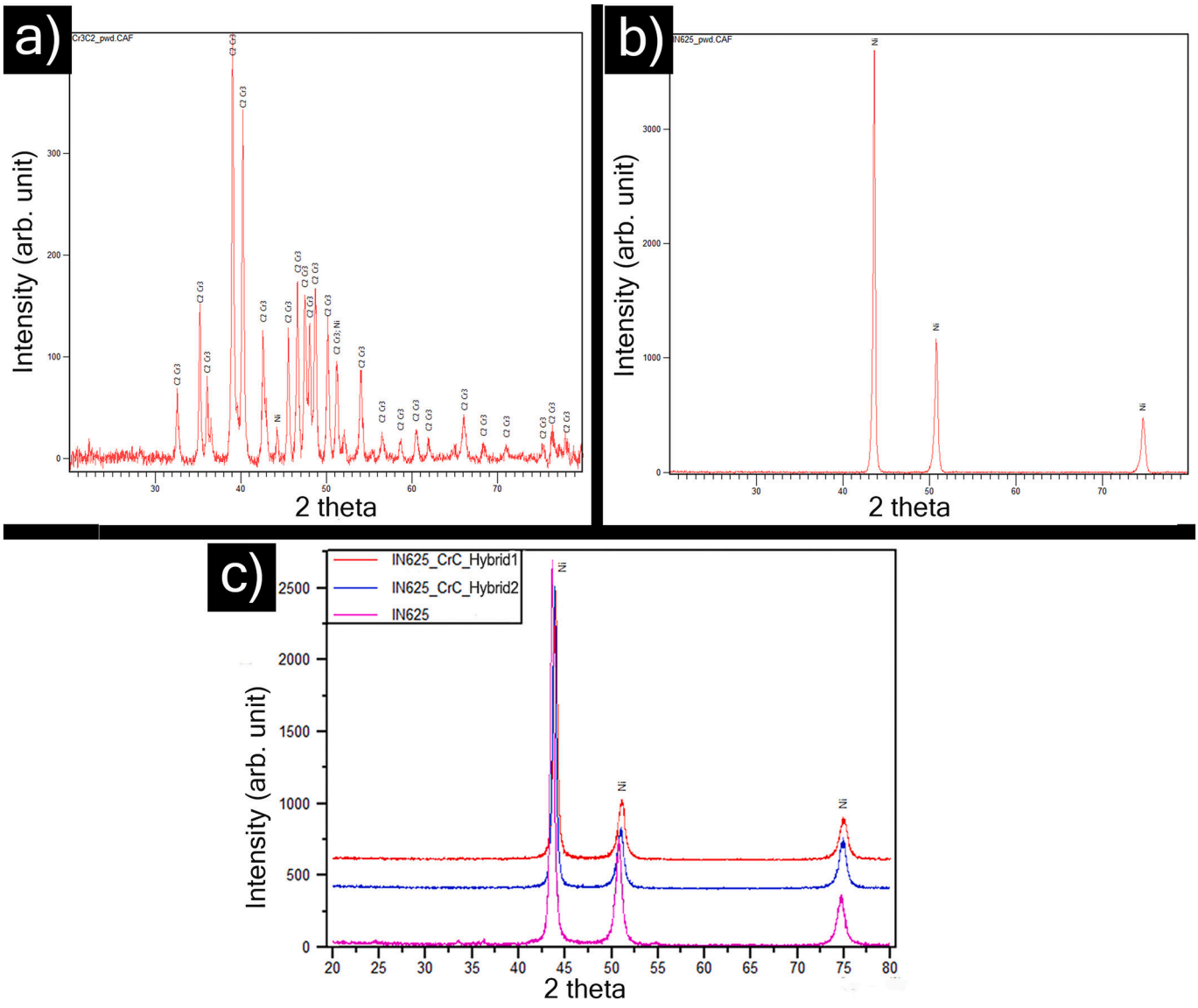

Fig. 8. XRD analysis of a) Cr_3C_2 feedstock b) IN-625 feedstock c) as-deposited coatings.

debris corresponds largely to splat boundary failure in IN625.

3.4.2.2. IN-625 coated specimen. The surface SEM analysis of IN-625 specimen showed a well-distinguished wear track, which was approximately 600 μm in width, according to Fig. 13(a). Furthermore, the wear track comprised bright and grey regions, similar to Hybrid-1 coating. Elemental EDS analysis of the bright region in the wear track at higher magnification showed the constituent alloy elements of IN-625

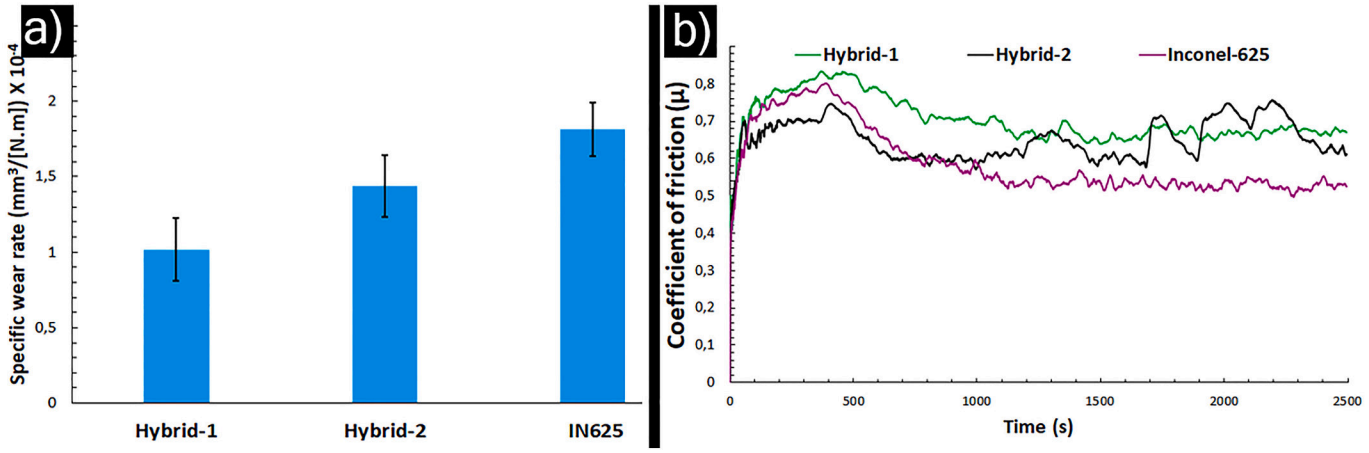

Fig. 9. a) Specific wear rates of the deposited coatings b) Coefficient of Friction (CoF) evolution of the as-deposited coatings.

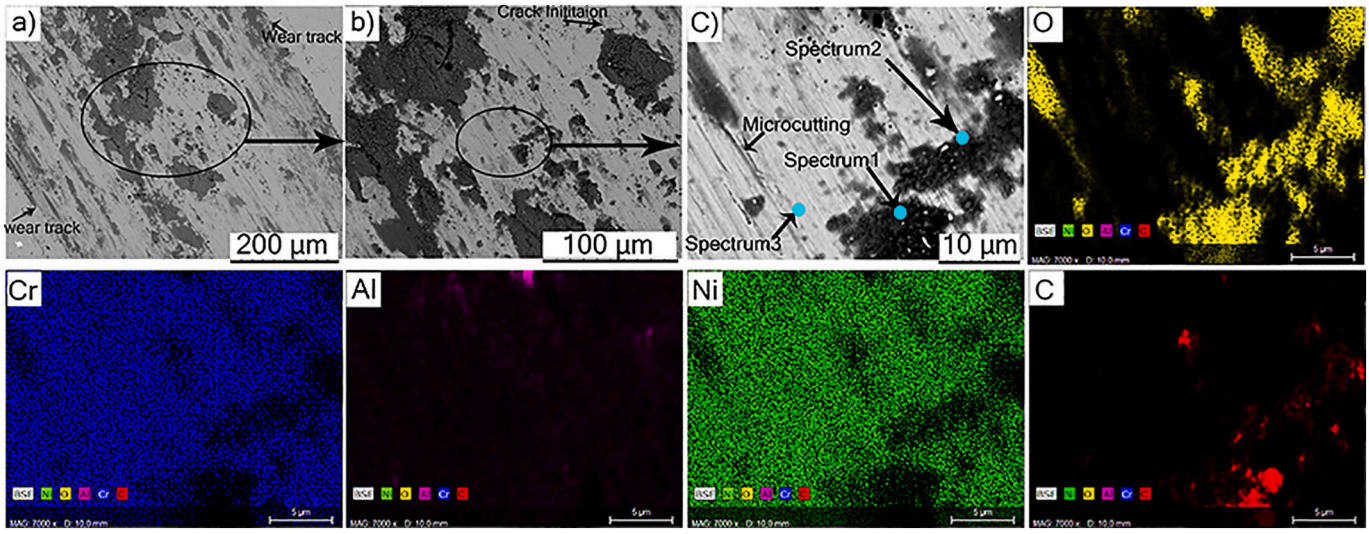

Fig. 10. Top surface SEM/EDS analysis of Hybrid-1 wear track a) low magnification micrograph b) high magnification micrograph c) higher magnification micrograph and its elemental maps.

Table IV
Quantitative (in wt%) EDS analysis of the worn Hybrid-1 coating (Spectrum1–3) and IN625 coatings (Spectrum 4–6).

Elements (wt%)	Spectrum-1	Spectrum-2	Spectrum-3	Spectrum-4	Spectrum-5	Spectrum-6
Ni	41.6	41.5	58.6	44.1	46.9	60.5
Cr	14.2	14.9	19.9	15.1	15.1	21.8
O	27.9	28.9	5.9	26.9	23	5.4
Mo	9.1	7.7	9.8	7.1	8.6	8.2
Nb	<1	<1	<1	<1	<1	<1
C	6.9	4.3	<1	<1	<1	<1
Fe	<1	<1	<1	<1	<1	<1
Al	<1	<1	<1	<1	<1	<1

i.e. 'Ni' and 'Cr' whereas the grey region showed 'O', 'Ni' and 'Cr', according to Fig. 13(b) and Table IV. It should be mentioned that the contrast was adjusted for the elemental maps shown. Furthermore, microcutting action of the wear debris could be seen in the bright region of the wear track, indicating the presence of abrasive wear mechanism. Traces of 'Al' were also observed in the coating wear track, indicating material transfer from the alumina ball surface to the coating. The worn ball surface in Fig. 14 also showed a distorted circular wear track, with a scar diameter (approximately 600 μm) similar to the wear track width of the IN-625 coated specimen. The wear debris particles showed fine and coarse size classes, as shown in Fig. 15(a). The coarser debris particles were approximately 50–150 μm in length whereas the fine particles were < 5 μm in length, according to Fig. 15(b). EDS elemental maps of the coarser wear debris at higher magnification showed presence of constituent alloying elements of IN-625. It is speculated that the larger debris could have been generated due to splat failure in the coating during the initial stages of the wear test. It should be mentioned that the particle size of the coarser debris that was possibly generated due to splat failure in IN-625 coating was 3–4 times higher than the coarser debris collected in the case of Hybrid-1 coating. On the other hand, the finer debris showed 'Cr', 'Ni' and 'O', indicating tribo-oxides that were also observed in the grey regions of the wear track. Furthermore, 'Al'

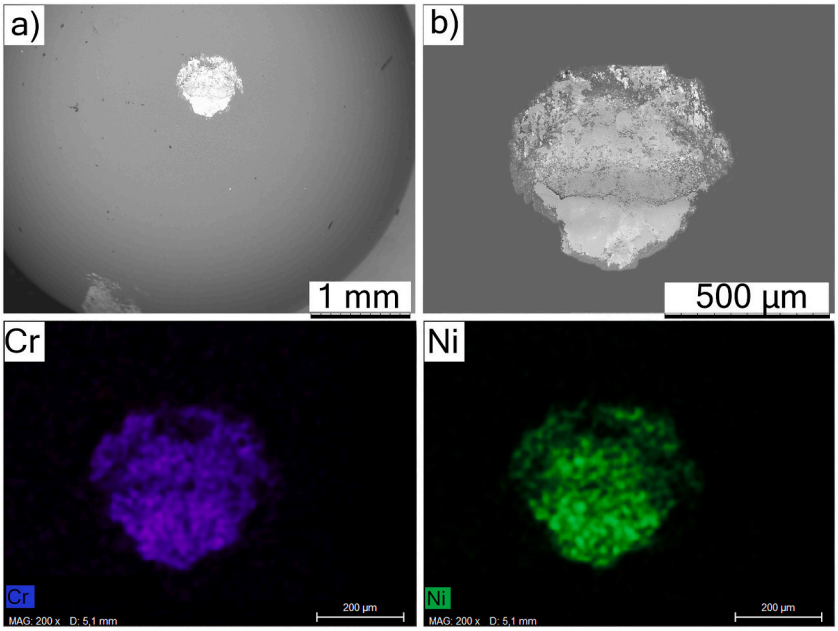

Fig. 11. SEM/EDS analysis of alumina ball used as counter surface to Hybrid-1 coating a) low magnification micrograph b) high magnification micrograph and its elemental map.

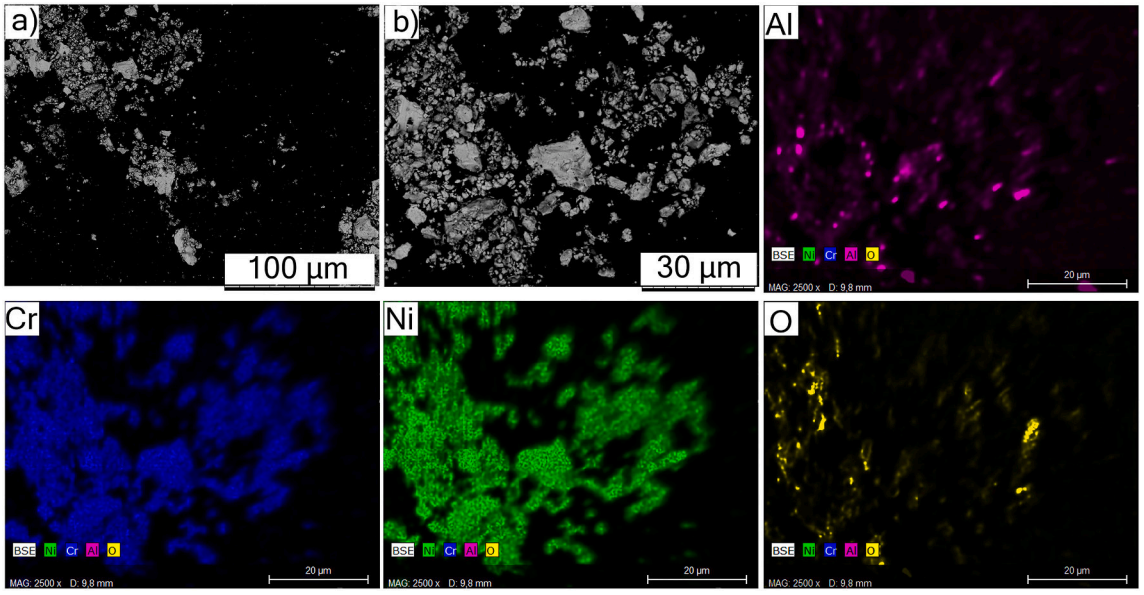

Fig. 12. SEM/EDS analysis of wear debris collected from Hybrid-1 coating a) low magnification micrograph b) high magnification micrograph and its elemental map.

was detected in the debris, indicating material loss from the alumina ball surface.

Based on the observed wear behavior of the conventional IN-625 coating and hybrid coatings (including ball wear and debris analysis), a schematic of their respective wear mechanisms is illustrated in Fig. 16. The conventional IN-625 coating showed the presence of several wear mechanisms such as tribo-oxidation, micro-cutting (abrasive wear), splat delamination etc. The hybrid coating also showed similar wear mechanisms. However, the Cr_3C_2 reinforcement in Hybrid-1 coating seemed to suppress material loss due to splat-boundary failure (based on debris analysis) as the reinforced carbide phase could have arrested the delamination cracks. Furthermore, the micro-cutting action of wear debris generated during the test on IN-625 splats was also minimized in hybrid coating as the harder carbide phase, while undergoing micro cracking, could have blunted the sharp abrasive particles and minimized the material loss. The above effects attributable to the presence of Cr_3C_2 phase resulted in lower wear rates for hybrid coatings compared to the conventional IN-625 coating.

3.5. Potentiodynamic polarization

The polarization response of all the coatings showed a typical Tafel behavior rather than a limiting diffusion current, see Fig. 17(a). This indicates the polarization was activation controlled rather than concentration polarization [34]. The anodic polarization response of Hybrid-1 and Hybrid-2 coatings showed a semi-passive region (−0.15 to

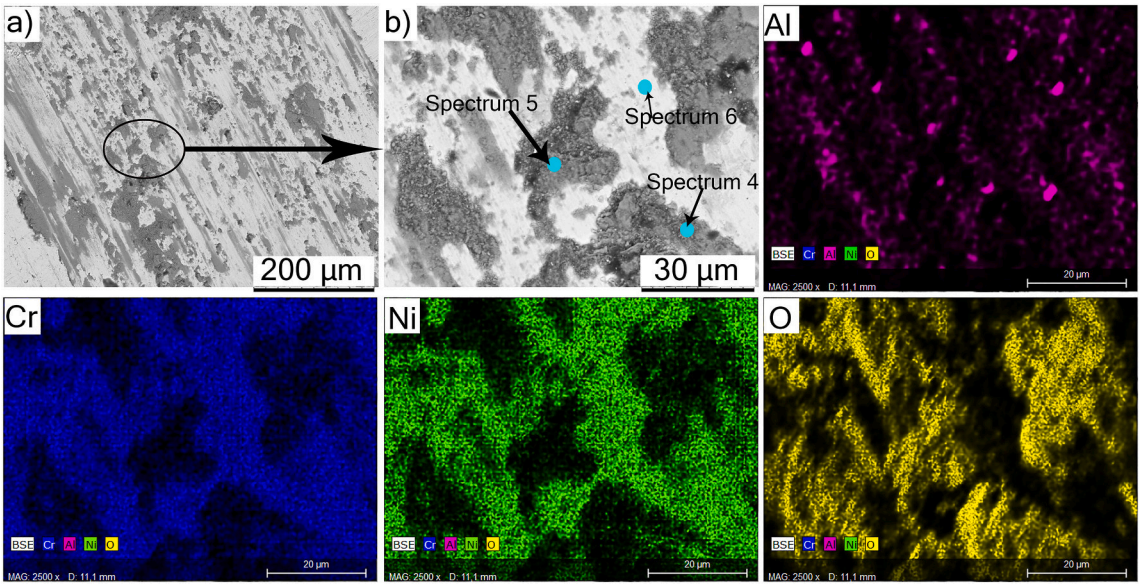

Fig. 13. Top surface SEM/EDS analysis of IN625 wear track a) low magnification micrograph b) high magnification micrograph and its elemental map.

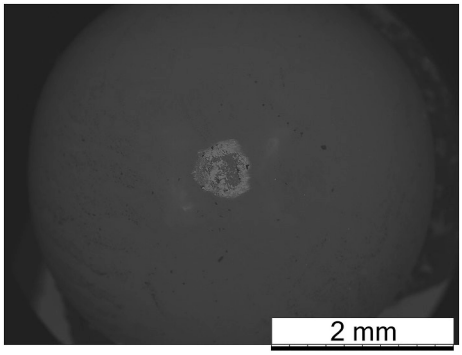

Fig. 14. SEM micrograph of worn alumina ball used as counter surface for IN625 coating.

0.5 V), where an increase in the applied potential did not significantly affect the current density. On the other hand, the IN-625 coating showed an independency of the applied potential only at higher current densities. In hybrid coatings, the semi-passive behavior at lower current density confirms that the presence of Cr_3C_2 phase aided in sustaining the corrosive environment. The polarization resistance (R_p) of Hybrid-1 (378 kΩ.cm^2) coating was higher than the IN-625 coating (88 kΩ.cm^2), indicating its higher resistance to corrosion, see Fig. 17(b). Corrosion potential (E_{corr}) for hybrid coatings was less negative, indicating their lower tendency to corrode compared to IN-625. Furthermore, Hybrid-1 coating with higher Cr_3C_2 content (approximately 4 vol %) showed higher corrosion resistance than the Hybrid-2 coating, which had Cr_3C_2 content of approximately 3 vol%.

The microstructural analysis and hardness results clearly indicate the presence of suspension derived carbides in the hybrid coatings. Co-deposition of harder reinforcement phase and a ductile matrix phase may lead to defects such as pores or cracks due to poor wetting of the harder phase by the ductile phase. However, no such defects were

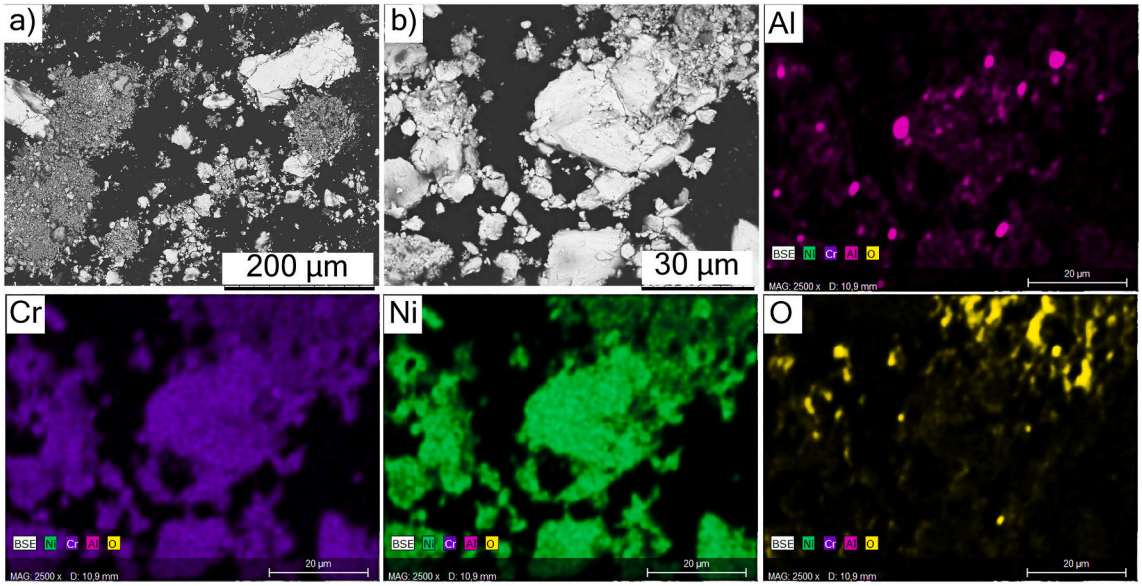

Fig. 15. SEM/EDS analysis of wear debris collected from IN625 coating a) low magnification micrograph b) high magnification micrograph and its elemental map.

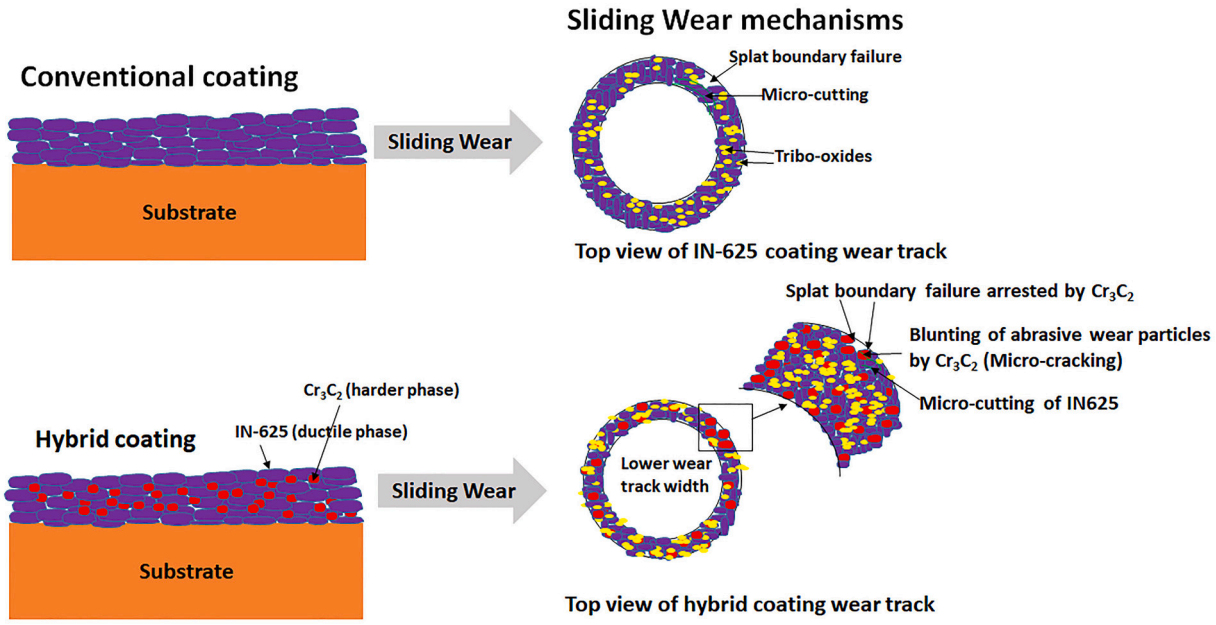

Fig. 16. Schematic illustration of the sliding wear mechanisms in a) IN-625 coating b) Hybrid coating.

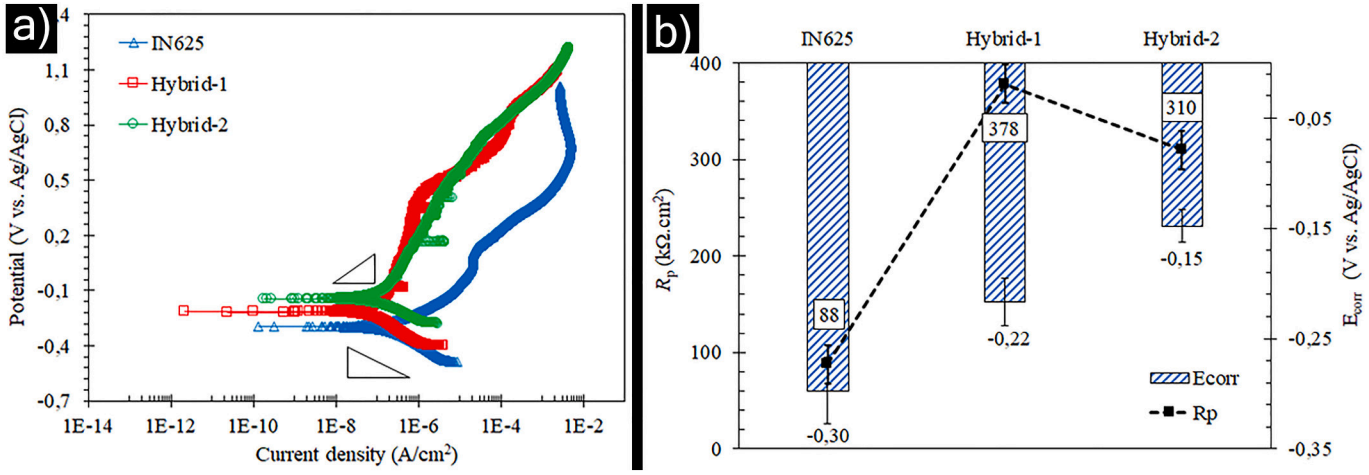

Fig. 17. Corrosion behavior of investigated coatings a) potentiodynamic polarization response b) polarization resistance (R_p) and corrosion potential (E_{corr}).

observed in the microstructural analysis of hybrid coatings. In fact, the porosity was shown to decrease with an increase in the reinforcement content in the coating. The improved wear performance results (lower wear rate) of hybrid coatings compared to conventional IN-625 coating concur with the above discussion related to absence of defects at the carbide/matrix interface. Furthermore, the debris particles collected from the hybrid coating showed lower particle size due to splat failure compared to conventional coating, indicating that the carbide phase effectively arrested the delamination cracks and minimized wear losses due to its defect-free IN-625/Cr_3C_2 interface. Although challenges still remain to improve the homogeneity in distribution of suspension fed feedstock due to pulsation encountered in the suspension feeding system, this work demonstrates that the concept of hybrid spraying can provide performance related benefits in several different applications where innovative functionalities are desirable. Tuning the pulsation damping of the suspension feeding device with the HVAF torch system back pressure (100 psi) is essential to enable the homogenous distribution of the suspension derived feedstock in the hybrid coating. Despite the technical challenges, as a case study, the wear performance of IN-625 was shown to improve with the addition of Cr_3C_2 by powder-suspension hybrid spraying without compromising its primary functionality, i.e. corrosion resistance. It should also be mentioned that the choice of the reinforcement phase and matrix phase needs to be carefully selected based on the factors such as service conditions (environments) etc. to exploit the benefits of hybrid spraying.

4. Conclusions

For the first time, this work demonstrated the possibility of utilizing a powder-suspension hybrid feedstock for HVAF spraying. In the present instance, this novel approach was harnessed to co-spray a Cr_3C_2 suspension with an IN-625 powder to achieve powder-suspension hybrid coatings with incorporated fine carbides. Microstructural analysis showed carbides distributed in the coating's bulk, although the engineering challenges related to overcoming the high back pressure in an HVAF to ensure reliable suspension feeding remain yet to be overcome. Sliding wear results clearly demonstrated higher wear resistance of hybrid coatings than conventional IN-625 coating. Hybrid coatings also showed improved corrosion resistance, indicating that the presence of Cr_3C_2 did not compromise the corrosion performance of IN-625.

Utilization of powder-suspension hybrid feedstock in a HVAF torch have significant potential implications in creating a new family of coatings that involve incorporation of a fine-sized, temperature sensitive second phase in conventional HVAF sprayed coatings. However, it is apparent that the challenge relating to suitable pulsation damping of the suspension feeding device to overcome the high back pressure typical of a HVAF torch system will have to be surmounted to ensure reliable suspension delivery for exploiting the above benefits.

CRediT authorship contribution statement

Satyapal Mahade: Writing – original draft, Conceptualization, Methodology, Investigation, Validation. **Lidia Baiamonte:** Investigation, Writing – review & editing. **Esmaeil Sadeghimeresht:** Investigation, Writing – review & editing. **Stefan Björklund:** Conceptualization, Methodology. **Francesco Marra:** Investigation, Writing – review & editing. **Shrikant Joshi:** Conceptualization, Methodology, Supervision, Funding acquisition, Writing – review & editing.

Declaration of competing interest

The authors declare that they have no known competing financial interests or personal relationships that could have appeared to influence the work reported in this paper.

Acknowledgements

We thank the Knowledge Foundation, Sweden, for its financial support to project HiPerCOAT (Dnr. 20180197). We also acknowledge help from Treibacher Industrie AG, Austria, for providing Chromium-Carbide suspension. Fruitful insights from Prof. Giovanni Pulci, Sapienza University of Rome, are also acknowledged.

References

[1] D. Tejero-Martin, M. Rezvani Rad, A. McDonald, T. Hussain, Beyond traditional coatings: a review on thermal-sprayed functional and smart coatings, J. Therm. Spray Technol. 28 (4) (2019) 598–644. Apr. https://doi.org/10.1007/s11666-019-00857-1.

[2] S. Joshi, P. Nylen, Advanced coatings by thermal spray processes, Technologies 7 (4) (2019) 79. Dec. https://doi.org/10.3390/technologies7040079.

[3] W. Fan, Y. Bai, Review of suspension and solution precursor plasma sprayed thermal barrier coatings, Ceram. Int. 42 (13) (2016) 14299–14312. Oct. https://doi.org/10.1016/j.ceramint.2016.06.063.

[4] J.O. Berghaus, B. Marple, C. Moreau, Suspension plasma spraying of nanostructured WC-12Co coatings, J. Therm. Spray Technol. 15 (4) (2006) 676–681. Dec. https://doi.org/10.1361/105996306X147072.

[5] K. VanEvery, et al., Column formation in suspension plasma-sprayed coatings and resultant thermal properties, J. Therm. Spray Technol. 20 (4) (2011) 817–828. Jun. https://doi.org/10.1007/s11666-011-9632-2.

[6] S. Björklund, S. Goel, S. Joshi, Function-dependent coating architectures by hybrid powder-suspension plasma spraying: injector design, processing and concept validation, Mater. Des. 142 (2018) 56–65. Mar. https://doi.org/10.1016/j.matdes.2018.01.002.

[7] J.W. Murray, A. Leva, S. Joshi, T. Hussain, Microstructure and wear behaviour of powder and suspension hybrid Al_2O_3–YSZ coatings, Ceram. Int. 44 (7) (2018) 8498–8504. May, https://doi.org/10.1016/j.ceramint.2018.02.048.

[8] S.V. Joshi, G. Sivakumar, T. Raghuveer, R.O. Dusane, Hybrid plasma-sprayed thermal barrier coatings using powder and solution precursor feedstock, J. Therm. Spray Technol. 23 (4) (2014) 616–624. Apr. https://doi.org/10.1007/s11666-014-0075-4.

[9] G. Sivakumar, S. Banerjee, V.S. Raja, S.V. Joshi, Hot corrosion behavior of plasma sprayed powder-solution precursor hybrid thermal barrier coatings, Surf. Coat. Technol. 349 (2018) 452–461. Sep. https://doi.org/10.1016/j.surfcoat.2018.06.021.

[10] F.J. Xu, Y.H. Lv, B.S. Xu, Y.X. Liu, F.Y. Shu, P. He, Effect of deposition strategy on the microstructure and mechanical properties of Inconel 625 superalloy fabricated by pulsed plasma arc deposition, Mater. Des. 45 (2013) 446–455. Mar. https://doi.org/10.1016/j.matdes.2012.07.013.

[11] T.E. Abioye, D.G. McCartney, A.T. Clare, Laser cladding of Inconel 625 wire for corrosion protection, J. Mater. Process. Technol. 217 (2015) 232–240. Mar. https://doi.org/10.1016/j.jmatprotec.2014.10.024.

[12] H. Edris, D.G. McCartney, A.J. Sturgeon, Microstructural characterization of high velocity oxy-fuel sprayed coatings of Inconel 625, J. Mater. Sci. 32 (4) (1997) 863–872. Feb. https://doi.org/10.1023/A:1018589230250.

[13] H.Y. Al-Fadhli, J. Stokes, M.S.J. Hashmi, B.S. Yilbas, The erosion–corrosion behaviour of high velocity oxy-fuel (HVOF) thermally sprayed inconel-625 coatings on different metallic surfaces, Surf. Coat. Technol. 200 (20) (2006) 5782–5788. May, https://doi.org/10.1016/j.surfcoat.2005.08.143.

[14] A.A. Boudi, M.S.J. Hashmi, B.S. Yilbas, HVOF coating of Inconel 625 onto stainless and carbon steel surfaces: corrosion and bond testing, J. Mater. Process. Technol. 155–156 (2004) 2051–2055. Nov. https://doi.org/10.1016/j.jmatprotec.2004.04.146.

[15] J. Mehta, V.K. Mittal, P. Gupta, Role of thermal spray coatings on wear, erosion and corrosion behavior: a review, Int. J. Appl. Sci. Eng. Technol. 20 (4) (2017) 445–452, https://doi.org/10.6180/jase.2017.20.4.05.

[16] O. Aranke, W. Algenaid, S. Awe, S. Joshi, Coatings for automotive gray cast iron brake discs: a review, Coatings 9 (9) (2019) 552. Sep. https://doi.org/10.3390/coatings9090552.

[17] H. Chen, I.M. Hutchings, Abrasive wear resistance of plasma-sprayed tungsten carbide–cobalt coatings, Surf. Coat. Technol. 107 (2) (1998) 106–114. Sep. https://doi.org/10.1016/S0257-8972(98)00581-7.

[18] S. Mahade, S. Björklund, S. Govindarajan, M. Olsson, S. Joshi, Novel wear resistant carbide-laden coatings deposited by powder-suspension hybrid plasma spray: characterization and testing, Surf. Coat. Technol. (2020) 126147. Jul. https://doi.org/10.1016/j.surfcoat.2020.126147.

[19] S. Mahade, K. Narayan, S. Govindarajan, S. Björklund, N. Curry, S. Joshi, Exploiting suspension plasma spraying to deposit wear-resistant carbide coatings, Materials 12 (15) (2019) 2344. Jan. https://doi.org/10.3390/ma12152344.

[20] D. Janicki, Laser cladding of Inconel 625-based composite coatings reinforced by porous chromium carbide particles, Opt. Laser Technol. 94 (2017) 6–14. Sep. https://doi.org/10.1016/j.optlastec.2017.03.007.

[21] Š. Houdková, Z. Česánek, E. Smazalová, F. Lukáč, The high-temperature wear and oxidation behavior of CrC-based HVOF coatings, J. Therm. Spray Technol. 27 (1) (2018) 179–195. Jan. https://doi.org/10.1007/s11666-017-0637-3.

[22] V. Matikainen, et al., A study of Cr_3C_2-based HVOF- and HVAF-sprayed coatings: microstructure and carbide retention, J. Therm. Spray Technol. 26 (6) (2017) 1239–1256. Aug. https://doi.org/10.1007/s11666-017-0578-x.

[23] F. Tarasi, M.S. Mahdipoor, A. Dolatabadi, M. Medraj, C. Moreau, HVOF and HVAF coatings of agglomerated tungsten carbide-cobalt powders for water droplet erosion application, J. Therm. Spray Technol. 25 (8) (2016) 1711–1723. Dec. https://doi.org/10.1007/s11666-016-0465-x.

[24] L. Ajdelsztajn, J.A. Ruud, Combustion Cold Spray, US20110293919A1, Dec. 01, 2011.

[25] L. Ajdelsztajn, J.A. Ruud, D.M. Gray, Coating Methods and Coated Articles, US20140175318, Mar.03, 2014.

[26] ImageJ, Softonic. https://imagej.en.softonic.com.

[27] G02 Committee, "Test method for wear testing with a pin-on-disk apparatus," J. ASTM Int. doi: https://doi.org/10.1520/G0099-17.

[28] E. Maleki, O. Unal, Optimization of shot peening effective parameters on surface hardness improvement, Met. Mater. Int. (2020), https://doi.org/10.1007/s12540-020-00758-x. Jun.

[29] V. Matikainen, G. Bolelli, H. Koivuluoto, P. Sassatelli, L. Lusvarghi, P. Vuoristo, Sliding wear behaviour of HVOF and HVAF sprayed Cr_3C_2-based coatings, Wear 388–389 (2017) 57–71. Oct. https://doi.org/10.1016/j.wear.2017.04.001.

[30] N. Vashishtha, S.G. Sapate, J.S. Gahlot, P. Bagde, Effect of tribo-oxidation on friction and wear behaviour of HVOF sprayed WC–10Co–4Cr coating, Tribol. Lett. 66 (2) (2018) 56. Mar. https://doi.org/10.1007/s11249-018-1006-1.

[31] N. Vashishtha, S.G. Sapate, Abrasive wear maps for high velocity oxy fuel (HVOF) sprayed WC-12Co and Cr_3C_2−25NiCr coatings, Tribol. Int. 114 (2017) 290–305. Oct. https://doi.org/10.1016/j.triboint.2017.04.037.

[32] N. Espallargas, J. Berget, J.M. Guilemany, A.V. Benedetti, P.H. Suegama, Cr_3C_2–NiCr and WC–Ni thermal spray coatings as alternatives to hard chromium for erosion–corrosion resistance, Surf. Coat. Technol. 202 (8) (2008) 1405–1417. Jan. https://doi.org/10.1016/j.surfcoat.2007.06.048.

[33] A. Dréano, S. Fouvry, G. Guillonneau, A tribo-oxidation abrasive wear model to quantify the wear rate of a cobalt-based alloy subjected to fretting in low-to-medium temperature conditions, Tribol. Int. 125 (2018) 128–140. Sep. https://doi.org/10.1016/j.triboint.2018.04.032.

[34] Denny A. Jones, Principles and Prevention Of Corrosion, 2nd ed, Upper Saddle River, NJ, 1995.